A 22 kW-85 kHz Three-phase Wireless Power Transfer System with 12 coils

Keisuke Kusaka
Dept. of Electrical, Electronics, and Information Engineering
Nagaoka University of Technology
Nagaoka, Japan
kusaka@vos.nagaokaut.ac.jp

Rintaro Kusui
Dept. of Electrical, Electronics, and Information Engineering
Nagaoka University of Technology
Nagaoka, Japan
kusui@stn.nagaokaut.ac.jp

Jun-ichi Itoh
Dept. of Electrical, Electronics, and Information Engineering
Nagaoka University of Technology
Nagaoka, Japan
itoh@vos.nagaokaut.ac.jp

Daisuke Sato
Nagaoka Motor Development Co., Ltd.,
Nagaoka, Japan
sato@nagaoka-md.co.jp

Shuichi Obayashi
Corporate Research & Development Center
Toshiba Corporation
Kawasaki, Japan
shuichi.obayashi@toshiba.co.jp

Masaaki Ishida
Corporate Research & Development Center
Toshiba Corporation
Kawasaki, Japan
masaaki1.ishida@toshiba.co.jp

***Abstract*—A 22-kW three-phase wireless power transfer (WPT) system with six primary coils and six secondary coils are proposed is developed in this paper. For the rapid charging of onboard batteries of electric vehicles (EVs), the output power of the WPT system should be increased. However, the increase of the WPT system may cause an increase in leakage magnetic flux. The leakage magnetic flux from the WPT system must comply with guidelines. The proposed WPT system with 12 solenoid coils, which are circularly placed, suppresses the leakage magnetic flux with two opposite solenoid coils which are differentially coupled. Moreover, the circularly placed coils cancel out the magnetic interference, which is caused by the coupling among the primary coils, and secondary coils. In this paper, first, the 22-kW three-phase WPT system is designed. Especially, the figure of coils, which achieves a minimum volume of the core, are determined with the cancellation capability of the magnetic interference. Then, the 22-kW WPT system is tested with a constant voltage load. The maximum efficiency of the proposed WPT system from a primary DC to a secondary DC side is 91.1% at an output power of 22 kW with a 400-V constant voltage load.**

Keywords—wireless power transfer, three-phase transmission, leakage magnetic flux

I. INTRODUCTION

In recent years, the number of electric vehicles (EVs) has been increasing for reducing the exhaust of NOx gas from vehicles for saving the environment. The travel distance of EVs is typically shorter than the conventional vehicles with gasoline or diesel because the power density of batteries is greatly smaller than the one of fossil fuel. Due to this limitation, EVs cannot be a substitute for conventional vehicles in terms of convenience because users are required to have a frequent charging.

One of the solutions for improving the convenience of the users of EVs is a wireless power transfer system (WPT) with magnetic induction [1–8]. The WPT system transmits power without any cable between the primary coil and the secondary coil. Thus, the users will start the charging of the onboard battery without an onerous connection of a charging cable.

Focusing on a wired battery charger, charging power of EVs has been increasing. Owing to the increase of battery capacity for achieving long travel distance, the battery capacity of EVs tends to be increased [9]. Based on this background, the charging power of the wired battery charger had been increased to 50 kW as the rapid charging in the standard published by CHAdeMO. Moreover, in the next generation standards, the charging power will be increased to 350 kW or 500 kW as an ultra-fast charging. Considering the increase of the charging power of the wired chargers, the output power of the WPT system should be increased for shortening charging time. In the standard, which will be published by SAE and ISO, the WPT system will be classified into five classes; WPT1–5, by the output power of the system. In the largest output power class; WPT5, the output power should be larger than 22 kW.

The increase of the output power may cause a problem of the leakage magnetic flux. The leakage magnetic flux must not affect any electronic devices, radio communications, and the human body. Thus the WPT system must comply with the guidelines, which are legislated in each area or country with considering the guidelines of ICNIRP and CISPR. As one of the solutions for reducing the leakage magnetic flux, the shielding with metal or magnetic material has been used [10–13]. However, the shielding method causes a large power loss due to the eddy current on the shield. In [14–16], the reduction method of the leakage magnetic flux using spread spectrum has been proposed. The radiation noise is reduced by randomly changing the output frequency of the inverter. By changing the transmission frequency, the peak of the radiation noise is suppressed in the frequency domain. However, the proposed method will not comply with the standard of the WPT for EVs. In [17], two-channel WPT system has been

This work is financially supported by Ministry of Internal Affairs and Communications, Japan.

proposed. The two-channel WPT system has two solenoid-type primary coils and two secondary coils, which are placed to cancel out the leakage magnetic flux, respectively. As the drawback of the cancellation of leakage magnetic flux, the main flux, which contributes transmitting power, is also interfered.

In this paper, the WPT system with 12-solenoid coils is proposed in order to reduce the radiation noise without any magnetic interference among the coils. The six primary coils are circularly placed to cancel out the magnetic flux due to the differential connection and magnetic interference among the primary coils. By adjusting the relationship of the magnetic coupling among the primary coils, the magnetic interference can be canceled out. The secondary coils are placed in the same manner. In the rest paper, first, the principle of the radiation noise cancellation is explained. Then, the 22-kW WPT system is designed considering the cancellation conditions. Finally, the 22-kW WPT system is performed.

II. Three-phase WPT System with 12 Coils

A. Circuit Configuration

Figure 1 shows the circuit configuration of the proposed three-phase WPT system. The proposed WPT system is based on a three-phase WPT system [18–20] with two coils on each phase. The three-phase transmission coils are connected in star-star windings. It should be noted that the star-star winding is used in this paper however the star-delta, delta-star, or delta-delta windings can be used for the system. Power is transmitted through the magnetic couplings M between the primary coils and the secondary coils, e.g., the coupling between L_{u1A} and L_{u2A}. The WPT system has the three-phase inverter, which is operated with a square wave operation, in the primary side and the three-phase diode bridge rectifier in the secondary side. In order to compensate the leakage inductance due to weak magnetic coupling, the six resonant capacitors C_{u1}, C_{v1}, C_{w1}, C_{u2}, C_{v2}, and C_{w2} are connected into the output of the three-phase inverter and the input of the three-phase inverter. The capacitors are selected to resonate with the self-inductance of each coil at the transmission frequency. Owing to the resonance, the inverter is operated in a zero-voltage switching (ZVS) condition when the output frequency is slightly higher than the resonant frequency because the parasitic capacitors of the MOSFETs, which will turn-on after the dead time, are discharged during the dead time by the circulating current [21].

Figure 2 shows the schematic of the transmission coils with the resonant capacitors. The solenoid coils are used for power transmission. The six solenoid coils are circularly placed. The pairs of two solenoid coils on the common phase are placed opposite and connected in series. The amplitude of the magnetic flux generated by two coils is the same because the inductance value is common on the primary coils and the secondary coils, respectively. The leakage magnetic flux is canceled out at a measuring point; it is typically 10 m from the system because the direction of the magnetic flux caused by the coils are opposite [17]. The coils on phase-v and phase-w are placed 120 degrees. Using the three-phase WPT system, the transmission power of each phase is divided into three. Thus, it is effective to reduce the duty of each coil in term of heat generation. However, the multiple coils cause a magnetic interference such as M_{an}, M_{bn}, and M_{cn} among the coils on the common side, i.e., primary side and the secondary side where

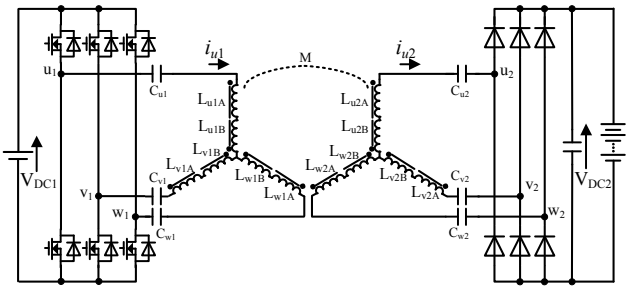

Fig. 1. Proposed three-phase wireless power trasnfer system with six primary coils and six secondary coils. The primary coils and the secondary coils are connected in star-star winding.

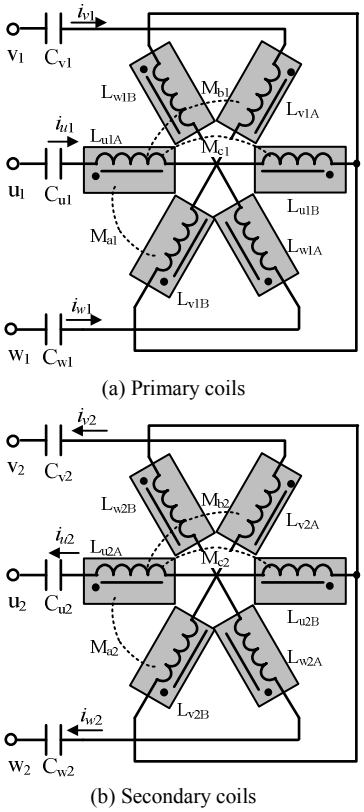

Fig. 2. Placement of 12-solenoid coils. The solenoid coils in common phase are placed opposite to each coil for noise reduction.

n represents the primary side as 1 and the secondary side as 2. The magnetic interference will be a reason for the power loss because the magnetic interference causes a circulating current on the windings due to the unnecessary induced voltage. In the proposed three-phase WPT system, the unnecessary induced voltage is canceled out by adjusting these unnecessary coupling as follow.

B. Cancellation of Magnetic Interference

In this section, the cancellation method of the magnetic interference, which will degrade the transmission efficiency, is explained. The induced voltage caused by the magnetic interference is canceled out by adjusting the coupling among the coils on the primary side and the secondary side.

The induced voltages on the 12 coils v_{unx}, v_{vnx}, and v_{wnx} are expressed as (1) considering the magnetic interference M_{an}, M_{bn}, and M_{cn} where x represents A or B. The variable L_{1Ys} is the self-inductance of each coil. Focusing on the first line of the matrix in (1), the induced voltage is expressed as (2).

$$\begin{pmatrix} v_{u1A} \\ v_{u1B} \\ v_{v1A} \\ v_{v1B} \\ v_{w1A} \\ v_{w1B} \\ v_{u2A} \\ v_{u2B} \\ v_{v2A} \\ v_{v2B} \\ v_{w2A} \\ v_{w2B} \end{pmatrix} = \begin{pmatrix} L_{1Ys} & M_{c1} & M_{b1} & M_{a1} & M_{b1} & M_{a1} & M & 0 & 0 & 0 & 0 & 0 \\ M_{c1} & L_{1Ys} & M_{a1} & M_{b1} & M_{a1} & M_{b1} & 0 & M & 0 & 0 & 0 & 0 \\ M_{b1} & M_{a1} & L_{1Ys} & M_{c1} & M_{b1} & M_{a1} & 0 & 0 & M & 0 & 0 & 0 \\ M_{a1} & M_{b1} & M_{c1} & L_{1Ys} & M_{a1} & M_{b1} & 0 & 0 & 0 & M & 0 & 0 \\ M_{b1} & M_{a1} & M_{b1} & M_{a1} & L_{1Ys} & M_{c1} & 0 & 0 & 0 & 0 & M & 0 \\ M_{a1} & M_{b1} & M_{a1} & M_{b1} & M_{c1} & L_{1Ys} & 0 & 0 & 0 & 0 & 0 & M \\ M & 0 & 0 & 0 & 0 & 0 & L_{2Ys} & M_{c2} & M_{b2} & M_{a2} & M_{b2} & M_{a2} \\ 0 & M & 0 & 0 & 0 & 0 & M_{c2} & L_{2Ys} & M_{a2} & M_{b2} & M_{a2} & M_{b2} \\ 0 & 0 & M & 0 & 0 & 0 & M_{b2} & M_{a2} & L_{2Ys} & M_{c2} & M_{b2} & M_{a2} \\ 0 & 0 & 0 & M & 0 & 0 & M_{a2} & M_{b2} & M_{c2} & L_{2Ys} & M_{a2} & M_{b2} \\ 0 & 0 & 0 & 0 & M & 0 & M_{b2} & M_{a2} & M_{b2} & M_{a2} & L_{2Ys} & M_{c2} \\ 0 & 0 & 0 & 0 & 0 & M & M_{a2} & M_{b2} & M_{a2} & M_{b2} & M_{c2} & L_{2Ys} \end{pmatrix} \frac{d}{dt} \begin{pmatrix} i_{u1} \\ -i_{u1} \\ i_{v1} \\ -i_{v1} \\ i_{w1} \\ -i_{w1} \\ i_{u2} \\ -i_{u2} \\ i_{v2} \\ -i_{v2} \\ i_{w2} \\ -i_{w2} \end{pmatrix} \quad (1)$$

$$v_{u1A} = L_{1Ys}\frac{di_{u1}}{dt} + M\frac{di_{u1}}{dt} - M_{a1}\left(\frac{di_{v1}}{dt} + \frac{di_{w1}}{dt}\right) + M_{b1}\left(\frac{di_{v1}}{dt} + \frac{di_{w1}}{dt}\right) - M_{c1}\frac{di_{u1}}{dt} \quad (2)$$

The first term of (2) is the induced voltage by the self-inductance and the second term is by the mutual coupling between the primary coil and the secondary coil, which transmits power. In contrast, the third to fourth terms are the interferences, which do not contribute to transmitting power. These terms should be canceled out. If the sum of the third to fourth terms can be zero, the proposed WPT system is as same as the single-phase WPT system with a primary coil and a secondary coil. In other words, the effect of other coils is not considered.

When the magnetic coupling between the primary coil and the secondary coil is the same, the three-phase current is equilibrium. Thus, (2) can be simplified as

$$v_{u1A} = L_{1Ys}\frac{di_{u1}}{dt} + M\frac{di_{u2}}{dt} - \omega I_{m1}\left\{M_{c1}\cos\omega t + \left(M_{a1} - M_{b1}\right)\cos\left(\omega t - \frac{2}{3}\pi\right) + \left(M_{a1} - M_{b1}\right)\cos\left(\omega t - \frac{4}{3}\pi\right)\right\} \quad (3),$$

where I_{m1} is the amplitude of the primary current.

Equation (3) shows that the unnecessary induced voltage can be canceled out by adjusting the relationship among M_{a1}, M_{b1}, and M_{c1} as shown by

$$M_{a1} = M_{b1} + M_{c1} \quad (4).$$

The self-inductance of the primary coils are common. Therefore the condition for the cancellation is expressed as

$$k_{a1} = k_{b1} + k_{c1} \quad (5)$$

with the magnetic coupling coefficient among the primary coils.

The cancellation condition of the induced voltage on the secondary side is introduced in the same manner as

$$k_{a2} = k_{b2} + k_{c2} \quad (6).$$

By satisfying both (5) and (6), the interference among the multiple coils is canceled out.

III. Design of 22-kW Prototype

A. Parameter Design

The transmission coils for designed in this section under the assumption that the magnetic interference is canceled out by satisfying (5–6).

The required inductance for each coil is calculated from an impedance matching condition. Thus, first, the equivalent AC resistance is calculated from a rated output power P_m and the DC voltage V_{DC2} on the secondary side. The AC resistance R_{eq} is expressed as (7) considering a derivation of an equivalent AC resistance of a single-phase rectifier [22]. The equivalent resistance is for one phase.

$$R_{eq} = \frac{8}{\pi^2}\frac{\left(V_{DC2}/2\right)^2}{P_m/3} = \frac{6}{\pi^2}\frac{V_{DC2}^2}{P_m} \quad (7)$$

The proposed system assumes to use a battery with a voltage of 200 to 400 V. Then, the system is designed to transmit 22 kW when the secondary DC voltage is 400 V. It means that the output power is derated when the secondary DC voltage is lower than 400 V.

Besides, the system is designed with an input power of 25 kW with a margin to ensure the input power of 22 kW considering the power loss of the system. Thus, the equivalent resistance is calculated with V_{DC2} = 400 V and P_m = 25 kW.

The secondary inductance is designed from the impedance matching condition. The impedance of the self-inductance should be equal to the equivalent AC resistance expressed by (7). In this consideration, parasitic resistances of the windings are ignored for simplicity. The secondary inductances for each phase are calculated by

$$L_{2Y} = L_{u2} = L_{v2} = L_{w2} = \frac{6}{\pi^2 k\omega}\frac{V_{DC2}^2}{P_m} \quad (8),$$

where ω (ω = 2πf) is the angular transmission frequency and k is the coupling coefficient between the primary coil and the secondary coil at the nominal position. The inductance calculated by (8) is for each phase. Thus, the inductance of each coil L_{2Ys} is the half of L_{2Y} because the proposed system has two coils in series in the phase. Note that, the transmission frequency f is the 85 kHz with considering the standardization of the WPT system by SAE and ISO.

The primary inductance is calculated from the voltage gain.

$$\frac{V_{DC2}}{V_{DC1}} = \sqrt{\frac{L_{2Y}}{L_{1Y}}} \quad (9)$$

From (8–9), the primary inductance is calculated by

$$L_{1Y} = L_{u1} = L_{v1} = L_{w1} = \frac{6}{\pi^2 k\omega}\frac{V_{DC1}^2}{P_m} \quad (10).$$

The inductance for each coil L_{1Ys} is half of L_{1Y} in the same manner to the secondary side.

Next, the resonant capacitors are selected. The resonant capacitors play a role as a compensation of the leakage inductances due to weak magnetic coupling k. In this paper, a series-series compensation [23] is used. In the series-series compensation, selecting the resonant capacitors to resonate with a self-inductance of each coil at the transmission frequency allows the efficient power transmission. Thus, the resonant capacitors for the primary side and the secondary side is calculated as

$$C_{u1Y} = C_{v1Y} = C_{w1Y} = \frac{1}{\omega^2 L_{1Y}} \quad (11)$$

$$C_{u2Y} = C_{v2Y} = C_{w2Y} = \frac{1}{\omega^2 L_{2Y}} \quad (12)$$

Note that, the output frequency is adjusted to be slightly higher than the resonant frequency, which is determined by (8, 10–12) for the ZVS of the inverter.

B. Size of coils

In this chapter, the shape of the transmission core is analyzed with the electromagnetic analysis. The figure of the core and the placement of coils are optimized for the minimum volume of the core with the capability of the radiation noise cancellation and the magnetic interference cancellation introduced in the previous chapter.

Figure 3 shows the schematic of the transmission coils for electromagnetic analysis. In this chapter, the transmission coil for a 22-kW wireless charger is analyzed and developed. First, the size of each coil is determined to obtain the required main coupling k for the power transmission. In this paper, the size of each transmission coils are x = 500, y = 250 mm for the main coupling k of 0.55 when the nominal transmission distance is d = 90 mm.

Then, the radius of the transmission coils is analyzed in order to satisfy the cancellation condition of the magnetic interference shown by (3). Figure 3 shows the analyzed model. The magnetic coupling among the coils on the common side mostly depends on the size of the ferrite core, and the placement of cores such as the radius r. The size of the ferrite core has been determined to obtain the required main coupling k. Thus, the cancellation conditions have to be satisfied by adjusting the distance r. Table I shows the effect of the radius r analyzed using an electromagnetic analysis. In this study, the radius r is designed to let the remaining magnetic interference k_a - k_b - k_c ten times smaller than the main coupling k. By increasing the radius r up to 750 mm, the remaining coupling is reducing because the effect of k_a is dominant. The transmission coils should be as small as possible as the cancellation condition is satisfied. Thus, in this paper, a radius r of 750 mm is selected from this consideration. Table II shows the results of the design consideration of the coils.

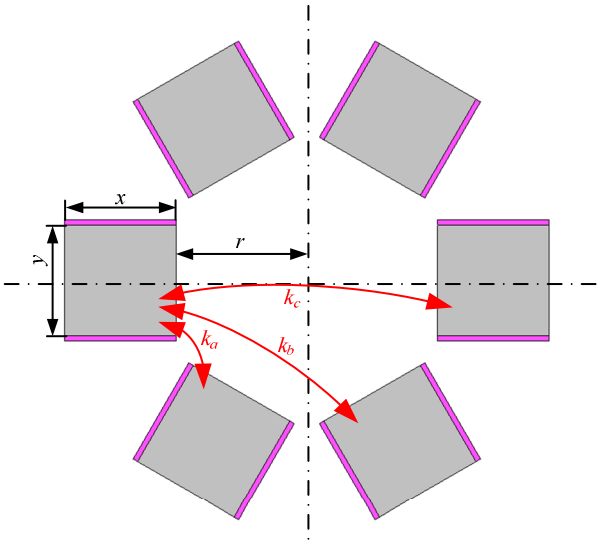

Fig. 3. Analytical model of transmission coils.

TABLE I. INTERFERENCE OF ELECTROMAGNETIC ANALYSIS.

Radius [mm]	Interference coupling			Cancellation
	k_a	k_b	k_c	k_a - k_b - k_c
700	0.100	0.0255	0.0175	0.0570
750	0.0893	0.0236	0.0163	0.0494
800	0.0824	0.0220	0.0152	0.0452

C. Power Loss

The power loss in the proposed system is calculated in this section.

1) Transmission coils

Assuming the unity power factor of the inverter output, the current on the primary coil at the rated power is calculated by

$$I_1 = \frac{P}{3V_1} = \frac{\pi P}{3\sqrt{2}V_{DC1}} \quad (13),$$

where V_{DC1} is the primary DC voltage, V_1 is the phase voltage of the inverter output with the square wave operation expressed as (14).

$$V_1 = \frac{\sqrt{2}}{\pi} V_{DC1} \quad (14)$$

The secondary current at the rated power is (15) in the same manner.

$$I_2 = \frac{\pi P}{3\sqrt{2}V_{DC2}} \quad (15)$$

The copper loss of each primary coils and secondary coils is calculated by

$$P_{1\_copper} = r_1 I_1^2 \quad (16),$$

$$P_{2\_copper} = r_2 I_2^2 \quad (17),$$

where r_1 and r_2 are the AC resistance of the transmission coils.

Besides, the iron loss is calculated from the magnetic flux density and the shape of coils. The iron loss is partially calculated with assuming the magnetic flux density is unity entire the ferrite core.

$$B_1 = \frac{L_{Y1s} I_1 + M I_2}{N_1 S_1} \quad (18),$$

$$B_2 = \frac{L_{Y2s} I_2 + M I_1}{N_2 S_2} \quad (19),$$

where N_n (n = 1, 2) is the number of turns and S_n is the cross-section of the ferrite core. The iron loss is read out from a datasheet of the magnetic material.

2) Inverter on the primary side

In the primary inverter, the switching loss and the conduction loss occur. The conduction loss of the MOSFETs in the primary inverter is calculated with assuming the constant equivalent resistance $r_{ds(\mathrm{on})}$.

$$P_{inv\_cond} = 6 r_{ds(on)} I_1^2 \quad (20)$$

The switching loss of the MOSFETs is calculated. The turn-on loss does not occur because the inverter is operated under the ZVS conditions. In contrast, turn-off loss occurs whereas the output current is sinusoidal. Assuming the sinusoidal current on the output of the inverter, the simultaneous current at the turn-off is approximately expressed by

$$i_{sw\_off} = \sqrt{2} I_1 \sin \omega T_d \quad (21),$$

where T_d is the dead time of the inverter. Thus the turn-off loss of the MOSFETs is expressed by

$$P_{1\_swoff} = 6 E_{off(isw\_off, V_{DC1})} \times f_{sw} \quad (22),$$

where E_{off} is the turn-off energy of MOSFETs.

3) Rectifier on the secondary side

In the rectifier on the secondary side, the conduction loss due to the diodes occurs. The current I_2 flows through two diodes during a half-period. Thus the sum of the conduction loss of the six diodes is calculated by (23).

$$P_{D\_cond} = 6 \frac{1}{T} \int_0^{\frac{T}{2}} V_F \sqrt{2} I_2 \sin \omega t dt = \frac{6\sqrt{2} V_F I_2}{\pi} \quad (23)$$

TABLE II. SPECIFICATION OF PROTOTYPE.

Parameters		Symbols	Value	
Input power		P_m	25	kW
Primary voltage		V_{DC1}	650	V
Secondary voltage		V_{DC2}	200-400	V
Transmission frequnecy		f	85	kHz
Air gap		g	90	mm
Core width		x	500	mm
Core length		y	250	mm
Core thickness		z	10	mm
Radius		r	750	mm
Number of turns	Primary	N_1	8	turn
	Secondary	N_2	5	turn
Self-inductance	Primary	L_{1Y}	21.8	μH
	Secondary	L_{2Y}	8.52	μH
Main coupling		k	0.55	
Core		PC95, TDK		
Litz wire		2UEWLZ 7×130 (ϕ0.1)		
MOSFETs		BSM300D12P2E001, ROHM		
Diodes		IDW40G120C5BFKSA1, Infineon Technologies		
Dead time		T_d	500	ns

IV. EVALUATION OF 22-KW PROTOTYPE

A. System Configuration

The 22-kW WPT system is tested in this chapter. Figure 4 shows the system configuration for the test. The input power is supplied through the variable transformer to adjust the input

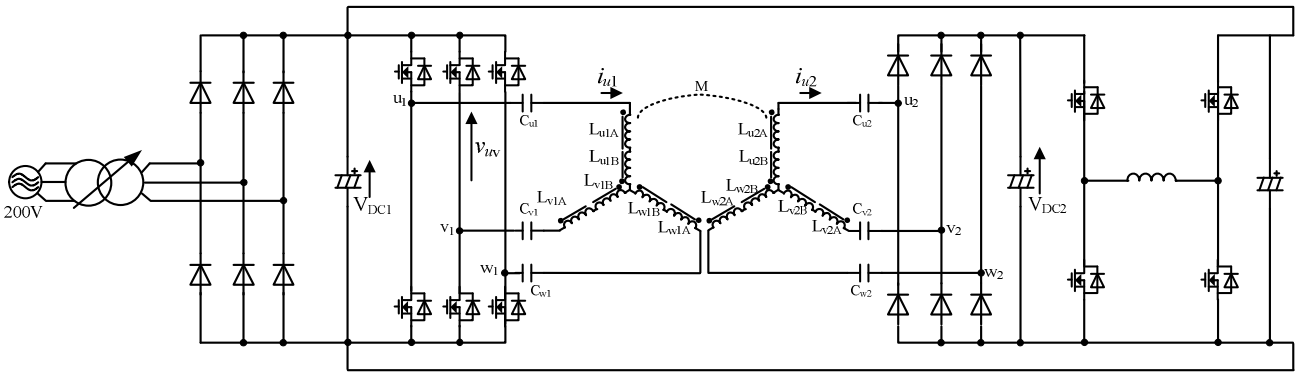

Fig. 4. System configuration of 22-kW test of the proposed WPT system. The output power ciculates through the buck and boost chopper. The primary DC voltage VDC1 is adjustable to control the power by the adjustable transformer at the input. The secondary DC voltage is also adjustable by the buck and boost chopper to emulate the constant voltage load such as batteries.

DC voltage. In the actual system, the primary DC voltage is adjustable by a PWM rectifier and a DC/DC converter for an output power control. However, it is omitted in this test for simplicity. The buck and boost chopper plays a role to circulate power from the output of the WPT system to the input. The secondary DC voltage V_{DC2} is adjustable from 200 to 400 V to emulate the constant voltage load such as onboard batteries. Due to this configuration, the input power source supplies only the power loss of the WPT system and the buck and boost chopper.

The transmission coils are developed according to the analysis in chapter III. The magnetic interference is k_{a1} = 0.0043, k_{b1} = 0.0026, k_{c1} = 0.0026, k_{a2} = 0.0090, k_{b2} = 0.0013, and k_c = 0.0006. The difference between the primary side and the secondary side is caused by a difference in the number of turns nevertheless the size of the ferrite core is the same.

B. Operation Waveforms

Figure 5 shows the operation waveforms when the primary DC voltage V_{DC1} is 650 V and the DC voltage on the secondary side is 400 V. The secondary DC voltage is controlled to emulate the constant voltage load by the buck and boost chopper. The output power is 22 kW. From Fig. 5 (a), it is shown that the proposed WPT system is operated with the resonant condition because the zero-cross of the primary current is synchronized with the voltage rise and fall of the inverter output voltage. From Fig. 5 (b), it is confirmed that the three-phase primary current is equilibrium. Fig. 5 (c) shows the three-phase output voltage of the inverter. The output voltage slowly step up or down by the ZVS operation.

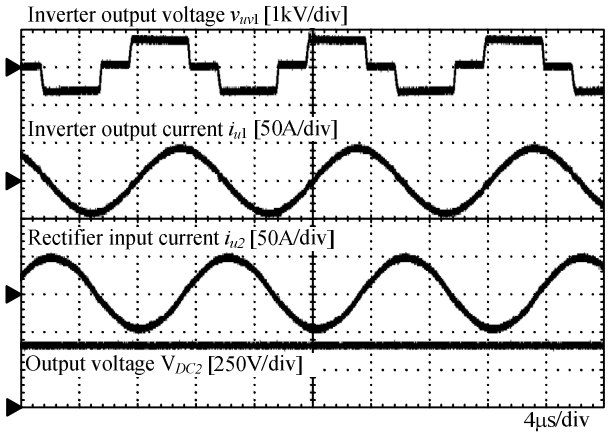

(a) Inverter output voltage, output current, rectifier input current, and output voltage

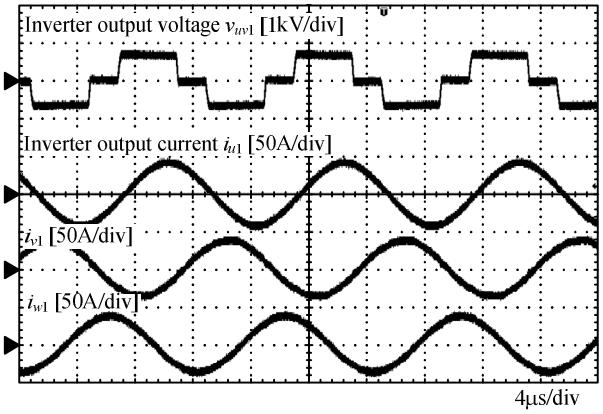

(b) Inverter output voltage, and output currents on each phase

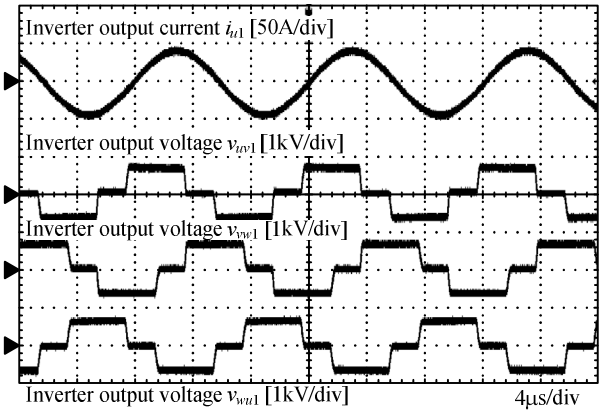

(c) Inverter output current, and inverter output voltages on each phase

Fig. 5. Operation waveforms of the proposed three-phase WPT system. The output power is 22 kW, primary DC voltage V_{DC1} is 650 V, secondary DC voltage is 400 V.

C. Efficinecy Evaluation

Figure 6 shows the efficiency characteristic of the proposed WPT system. The efficiency from the primary DC V_{DC1} to the secondary DC side V_{DC2} is measured. It means that the DC-to-DC efficiency take into account the power losses of the inverter and the rectifier. The primary DC voltage V_{DC1} is adjusted to control the output power. By contrast, the

secondary voltage is changed to 200, 300, and 400 V to emulate the constant voltage load. The maximum output power is derated by the secondary current on the coils and the diode bridge rectifier. The maximum efficiency is 91.1% at an output power of 22 kW, 91.3% at 10 kW, and 91.3% at 5.0 kW when the secondary DC voltage is 400, 300, and 200V, respectively.

Figure 7 shows a breakdown of the power loss when the primary DC voltage is 650 V, the secondary DC voltage is 400 V, the output power is 22 kW. The power loss is calculated with the equations in chapter III. The power loss measured through the experiment is 2.16 kW. On the other hand, the sum of the calculated power loss is 1.90 kW. The error between the experiment and the calculation is 262 W where it is 1.2% of the output power. In other words, the estimated efficiency by the calculation is 92.0% as against a measured efficiency of 91.1%.

In the calculation, the power loss is dominated by the conduction loss of the MOSFETs on the primary inverter. It accounts for 26.9% of the total loss. The second largest power loss is the copper loss of the secondary coil because the large current flows on the secondary coil because the secondary DC voltage is lower than the primary DC voltage. It is 22.3% of the total loss.

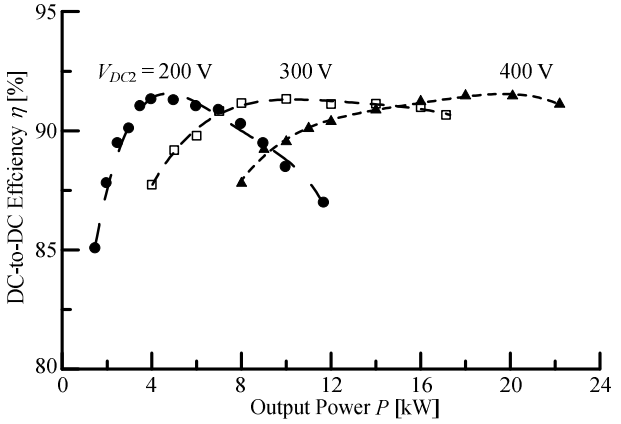

Fig. 6. Efficiency characteristic with different secondary DC voltage. The secondary DC voltage is changed from 200 V to 400 V. The DC-to-DC efficiency consists of the power loss of the primary inverter, the 12 coils, and the rectifier.

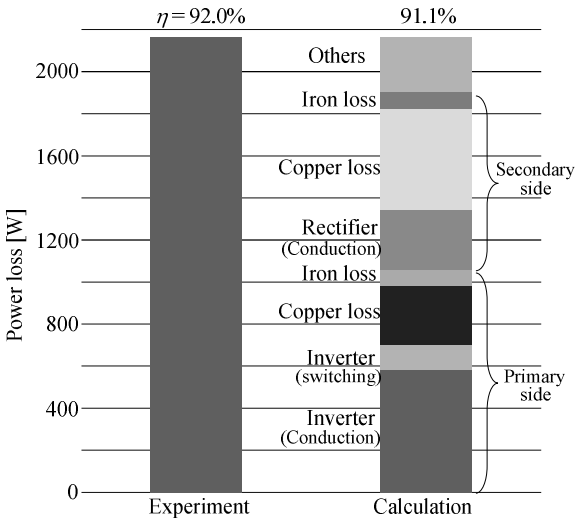

Fig. 7. Power loss separation of 22-kW prototype.

V. Conclusion

In this paper, the 22-kW three-phase WPT system with 12 coils has been developed for a rapid charger of EVs. The proposed WPT system transmits power through 12-solenoid coils, which are circularly placed. The pairs of two coils, which are connected in series, in the common phase are placed opposite. Thus, the radiation noise will be canceled out at the measuring point of emission. However, not only the proposed system has a problem, but also the WPT system with multiple coils. The magnetic interference among the coils degrades the transmission efficiency. In the proposed WPT system, the magnetic interference is canceled out by using three-phase transmission and adjusting the relation between the coils. Specifically, the coupling among the coils is adjusted to satisfy $k_{an} = k_{bn} + k_{cn}$. The proposed 22-kW WPT system is tested with a constant voltage load. The maximum efficiency of the proposed system from the primary DC side to the secondary DC side is 91.1% with the constant output voltage of 400 V when the output power is 22 kW. The power loss at the rated power is dominated by the conduction loss of the primary inverter. It accounts for 26.9% of the total loss.

In future work, radiation noise emission from the proposed three-phase WPT system will be measured. Moreover, system efficiency will be improved by the optimization of the system.

References

[1] R. Bosshard, J. W. Kolar, J. Mühlethaler, I. Stevanović, B. Wunsch and F. Canales, "Modeling and η-α–Pareto Optimization of Inductive Power Transfer Coils for Electric Vehicles," IEEE Journal of Emerging and Selected Topics in Power Electronics, Vol. 3, No. 1, pp. 50-64 (2015)

[2] F. Musavi, M. Edington and W. Eberle, "Wireless power transfer: A survey of EV battery charging technologies," 2012 IEEE Energy Conversion Congress and Exposition (ECCE), pp. 1804-1810 (2012)

[3] S. Li, C. C. Mi, "Wireless Power Transfer for Electric Vehicle Applications," IEEE Journal of Emerging and Selected Topics in Power Electronics, Vol. 3, No. 1, pp. 4-17 (2015)

[4] G. Lovison, T. Imura, H. Fujimoto, Y. Hori, "Secondary-side-only Phase-shifting Voltage Stabilization Control with a Single Converter for WPT Systems with Constant Power Load," IEEJ Journal of Industry Applications, Vol. 8, No. 1, pp. 66-74 (2019)

[5] V. Doan, H. Fujimoto, T. Koseki, T. Yasuda, H. Kishi, T. Fujita, "Simultaneous Optimization of Speed Profile and Allocation of Wireless Power Transfer System for Autonomous Driving Electric Vehicles," IEEJ Journal of Industry Applications, Vol. 7, No. 2, pp. 189-201 (2018)

[6] K. Kusaka, J. Itoh, "Development Trends of Inductive Power Transfer Systems Utilizing Electromagnetic Induction with Focus on Transmission Frequency and Transmission Power," IEEJ trans. on Industry Applications, Vol. 6, No. 5, pp. 328-339 (2017)

[7] T. Koyama, K. Umetani, E. Hiraki, "Design Optimization Method for the Load Impedance to Maximize the Output Power in Dual Transmitting Resonator Wireless Power Transfer System," Vol. 7, No. 1, pp. 49-55 (2019)

[8] G. Lovinson, D. Kobayashi, M. Sato, T. Imura, Y. Hori, "Secondary-side-only Control for High Efficiency and Desired Power with Two Converters in Wireless Power Transfer Systems," Vol. 6, No. 6, pp. 473-481 (2017)

[9] A. Kurokawa, M. Yano, Y. Matsuoka, “Hybrid vehicles, electric vehicles, fuel cell electric vehicles, traction motors,” Journal of Society of Automotive Engineers of Japan, Vol. 72, pp. 90-100 (2018)

[10] M. Jo, Y. Sato, Y. Kaneko, S. Abe, “Methods for Reducing Leakage Electric Field of a Wireless Power Transfer System for Electric Vehicles,” IEEE Energy Conversion Congress and Exposition (ECCE) 2014, pp. 1762-1769 (2014)

[11] H. Kim, J. Cho, S. Ahn, J. Kim, J. Kim, “Suppression of Leakage Magnetic Field from a Wireless Power Transfer System using Ferrimagnetic Material and Metallic Shielding,” IEEE International Symposium on EMC, 978-1-4673-2061-0, pp.640-645 (2012)

[12] T. Campi, S. Cruciani, M. Feliziani, “Magnetic Shielding of Wireless Power Transfer Systems,” IEEE International Symposium on EMC, 15A-H1, pp.422-425 (2014)

[13] K. Maikawa, K. Imai, Y. Minagawa, M. Arimitsu, H. Iwao, “Magnetic Field Reduction Technology of Wireless Charging System,” Society of Automotive Engineers of Japan 2013, No. 110-13 (2013)

[14] K. Inoue, K. Kusaka, J. Itoh, “Reduction in Radiation Noise Level for Inductive Power Transfer Systems Using Spread Spectrum Techniques,” IEEE Trans. on Power Electronics, Vol. 33, No. 4 pp. 3076-3085 (2017)

[15] K. Kusaka, K. Inoue and J. Itoh, “Radiation noise reduction using spread spectrum for inductive power transfer systems considering misalignment of coils,” 2017 IEEE Energy Conversion Congress and Exposition (ECCE) 2017, pp. 5507-5514 (2017)

[16] K. Inoue, K. Kusaka and J. Itoh, “Reduction on radiation noise level for inductive power transfer systems with spread spectrum focusing on combined impedance of coils and capacitors,” 2016 IEEE Energy Conversion Congress and Exposition (ECCE), pp. 1-8 (2016)

[17] T. Shijo, K. Ogawa, M. Suzuki, Y. Kanekiyo, M. Ishida, S. Obayashi, “EMI Reduction Technology in 85 kHz Band 44 kW Wireless Power Transfer System for Rapid Contactless Charging of Electric Bus”, IEEE Energy Conversion Congress & Expo 2016, No. EC-0641 (2016)

[18] Y. Tanikawa, M. Kato, T. Imura, Y. Hori, “Experiment of magnetic resonant coupling three-phase wireless power transfer,” 2013 World Electric Vehicle Symposium and Exhibition (EVS27), pp. 1-8 (2013)

[19] M. Kim, H. Kim, D. Kim, Y. Jeong, H. Park and S. Ahn, “A Three-Phase Wireless-Power-Transfer System for Online Electric Vehicles With Reduction of Leakage Magnetic Fields,” IEEE Transactions on Microwave Theory and Techniques, Vol. 63, No. 11, pp. 3806-3813 (2015)

[20] C. Song, H. Kim, D. H. Jung, K. Yoon, Y. Cho, S. Kong, Y. Kwack, J. Kim, “Three-phase magnetic field design for low EMI and EMF automated resonant wireless power transfer charger for UAV,” 2015 IEEE Wireless Power Transfer Conference (WPTC), pp. 1-4 (2015)

[21] K. Liu, F. C. Y. Lee, “Zero-voltage switching technique in DC/DC converters,” IEEE Transactions on Power Electronics, Vol. 5, No. 3, pp. 293-304 (1990)

[22] R. L. Steigerwald, “A Comparison of Half-Bridge Resonant Converter Topologies,” IEEE Trans. on Power Electronics, Vol. 3, No. 2, pp. 174-182 (1988)

[23] Y. Sohn, B. H. Choi, E. S. Lee, G. C. Lim, G. Cho, C. T. Rim, “General Unified Analyses of Two-Capacitor Inductive Power Transfer Systems: Equivalence of Current-Source SS and SP Compensations,” IEEE Transactions on Power Electronics, Vol. 30, No. 11, pp. 6030-6045 (2015)